ACS APPLIED MATERIALS & INTERFACES

Article

Interference-Free Micro/Nano-particle Cell Engineering Using High-Throughput Microfluidic Separation

David Yeo, Christian Wiraja, Yingying Zhou, Huimin Tay, Hanwei Hou, and Chenjie Xu

ACS Appl. Mater. Interfaces, **Just Accepted Manuscript** • DOI: 10.1021/acsami.5b06167 • Publication Date (Web): 01 Sep 2015

ACS Publications

ACS Applied Materials & Interfaces is published by the American Chemical Society.
1155 Sixteenth Street N.W., Washington, DC 20036

Interference-Free Micro/Nano-particle Cell Engineering Using High-Throughput Microfluidic Separation

David C. Yeo,† Christian Wiraja, † Yingying Zhou, † Hui Min Tay,‡ Han Wei Hou,‡ Chenjie Xu , † , §,**

† School of Chemical & Biomedical Engineering, Nanyang Technological University, 62 Nanyang Drive, Singapore 637459, ‡ Lee Kong Chian School of Medicine, Nanyang Technological University, 50 Nanyang Drive, Singapore 637553, § NTU-Northwestern Institute of Nanomedicine, Nanyang Technological University, 50 Nanyang Avenue, Singapore 639798

KEYWORDS: cell engineering, cell separation, nanoparticle, Dean Flow Fractionation, microfluidics

ABSTRACT. Engineering cells with active-ingredient-loaded micro/nano-particles is becoming increasingly popular for imaging and therapeutic applications. A critical yet inadequately addressed issue during its implementation concerns the significant amounts of particles that remain unbound following the engineering process, which inadvertently generates signals and impart transformative effects onto neighboring non-target cells. Here we demonstrate that those unbound micro/nano-particles remaining in solution can be efficiently separated from the particle-labeled cells by implementing fast, continuous and high-throughput Dean Flow

Fractionation (DFF) microfluidic device. As a proof-of-concept, we applied the DFF microfluidic device for buffer exchange to sort labelled suspension cells (THP-1) from unbound fluorescent dye and dye-loaded micro/nano-particles. Compared to conventional centrifugation, the depletion efficiency of free dyes or particles was improved 20 fold and the mislabeling of non-target bystander cells by free particles was minimized. The microfluidic device was adapted to further accommodate heterogeneous-sized mesenchymal stem cells (MSCs). Complete removal of unbound NPs through DFF microfluidics led to the usage of engineered MSCs without exerting off-target transformative effects on the functional properties of neighboring endothelial cells. Apart from its effectiveness in removing free particles, this strategy is also efficient and scalable. It could continuously process cell solutions with concentrations up to 10^7 cells/mL (cell densities commonly encountered during cell therapy) without the observable loss of performance. Successful implementation of this technology is expected to pave the way for interference-free clinical application of micro/nano-particle engineered cells.

INTRODUCTION

Engineering cells using agent-loaded micro/nano-particles is a simple, genomic integration-free and versatile method to imbue bioimaging capability and/or to augment/supplement its native therapeutic properties. Labeling cells with particle-based contrast agents enables the optimization of cell administration by monitoring cell biodistribution, status/function and other activities post-transplantation.[1-3] For example, magnetic resonance imaging (MRI) could successfully ascertain the accurate injection delivery of super-paramagnetic iron oxide (SPIO) labeled dendritic cells as well as its migration behavior within cancer patient's lymph nodes.[4] Furthermore, engineering cells with microparticles containing transformative agents such as doxorubicin and antibodies respectively improve anti-cancer efficacy through targeted drug delivery and the manipulation of

intracellular kinase activity[5-6] Such means of cellular modification typically utilizes either physical or chemical means to decorate various cell locations such as the plasma membrane or the cytoplasm.[7] Excess concentration levels of particles are usually supplied to saturate binding site(s), leaving significant quantities of unbound particles remaining in solution post-labeling. Remnant free particles confound precise identification of particle-engineered cells or potentially complicate therapeutic outcomes.[8-9] Free particles even cause cytotoxicity and interfere with other cells. Even bioimaging agents that are FDA-approved (e.g. indocyanine green) for various applications can be cytotoxic to certain cell-types like retinal pigment epithelium.[10] Exposure to either transformative agents (e.g. growth factors, corticosteroids etc.) at excessively high concentration levels or misdirected exposure (acting on non-target cells) may induce unintended consequences (as shown herein). Even particulate carriers comprising 'biocompatible' materials (e.g. PLGA) can incite potent immune cell responses under certain conditions.[11] Size, morphology, surface characteristics and geometry are further particle design characteristics that determine toxicity profile.[12] Furthermore, individuals suffering from autoimmune diseases (e.g. rheumatoid arthritis) have greater proportion of T helper Type I cells which potentially delays nanoparticle systemic clearance.[13] Thus, removing free particles minimizes toxicity profile and the risk of misdirected exposure to agent-loaded particles.

Conventional washing procedures do not always purify engineered cells completely.

Conventional gradient centrifugation can separate engineered cells from free particles but is a laborious and fragmented process performed in batch. Moreover, shear stresses experienced by cells during high-speed centrifugation and the constituents of the density gradient medium may compromise cell integrity and/or influence cell behavior.[14] Microfluidics separation technologies is an attractive alternative and in recent years, several microfluidic strategies for continuous flow

solution exchange have been reported such as deterministic lateral displacement (DLD)[15], dielectrophoresis[16-17], acoustophoresis[18] and inertial microfluidics[19-21]. DLD microdevices have good separation resolution but suffer from low throughput (<1 μLmin^{-1}) and are prone to clogging issues within the micro-pillar array. Similarly, dielectrophoresis-based methods are low throughput (~1-3 μLmin^{-1}) and require differences in intrinsic dielectrophoretic cell phenotypes or additional cell labelling steps to achieve separation[16]. Acoustophoretic particle washing achieves high buffer exchange efficiency (~99.98%) but is limited by low particle recovery (~75%).[18] A more promising approach involves inertial microfluidics - the lateral migration of particles or cells across streamlines to focus at distinct positions due to dominant lift forces (FL) at high Reynolds number (*Re*)[22-24] and have been employed for buffer exchange applications by switching particle focusing position in micro-channels of different aspect ratios[19] or inducing inertial flow deformation using micro-pillars.[20-21] However, these techniques have poor solution exchange performance (~10-30% contaminant solution remains) as the separated cells usually remain close to the boundary between original and new buffer solutions.[19-21] More importantly, size distribution of target cells has to be similar to achieve precise inertial focusing and separation from original buffer solution and would be an issue especially when processing heterogeneous-sized cell types such as mesenchymal stem cells (MSCs).[25]

Herein, we introduce a novel approach to efficiently remove unbound particles (<2 μm) from particle-engineered cells with high heterogeneity in cell size (10-30μm) in a continuous and high throughput manner (Figure 1). This is based on an inertial microfluidics technique termed Dean Flow Fractionation (DFF) previously developed for isolating circulating tumor cells (CTCs) in spiral micro-channels[26]. Specifically, the mixture of engineered cells and free particles post-labeling is injected into one of two inlets of a spiral microfluidic device at high throughput (~10^{6}-

^{7}/mL) while another inlet runs fresh buffer solution. Under the influence of Dean Drag forces in spiral channels, cells in the mixture migrate laterally from the outer wall towards inner wall. The larger-sized cells experience stronger inertial lift forces and focus near the micro-channel inner wall while the (smaller) free particles recirculate to the outer wall following the completion of a full "Dean-cycle". This facilitates the collection of a pure population of particle-engineered cells into the cell outlet suspended in buffer solution while unbound free particles are retrieved from the waste channel.

DFF buffer exchange microfluidic technology was first applied to sort labeled suspension cells (THP-1) from unbound fluorescent dye and/or micro/nano-particles. Superior separation performance compared to conventional centrifugation was observed and the mislabeling of non-target bystander cells by the free particles was observed to be minimal. The microfluidic device was then adapted to further accommodate heterogeneous-sized mesenchymal stem cells (MSCs). By completely removing free particles, engineered MSCs did not exert off-target transformative effects on neighboring endothelial cells. This new cell purification strategy facilitates large volume cell sorting and can process up to 10 million cells/mL – cell densities amenable for regenerative medicine applications.

RESULTS AND DISCUSSIONS

Design Principles of DFF Microfluidic Purification. Fluid flow through a spiral channel generates centrifugal acceleration radiating outward, leading to two counter-rotating Dean vortices forming in the top and bottom halves of the channel.[27] These transverse Dean Flow patterns impose additional lateral drag forces (F_D) that provide superior separation resolution,[28-30] since both inertial lift and drag forces (F_L and F_D) scale non-linearly with particle size. Their

superposition (F_L/F_D) determines the particle's equilibrium axial position along the micro-channel cross-section.

Based on this theory, a spiral DFF device was fabricated using polydimethylsiloxane (PDMS) consisting of a 2-inlet, 2-outlet spiral microchannel (500 μm (w) × 115 μm (h)) with a total length of ~10 cm (Figure 1A). This length was used to ensure sufficient time for complete Dean migration and recirculation of nanoparticles towards the outer wall as discussed previously.[26] Because the equilibrium position of particles depends on the shortest channel dimension (micro-channel height, h) due to varying shear rates across the channel cross-section (particle size (a_p)/h > 0.07), the channel height was fixed at 115 μm so that cells (typical size ~15 μm) can experience inertial focusing (a_p/h ~ 0.1) and equilibrate at a position of <20% width (<100 μm) from the inner wall.[29, 31] At these flow conditions, particles were similarly focused within 20% (<100 um) of the opposite channel, adjacent to the outer wall. During operation, a mixture of cells and particles were perfused into the outer wall inlet (75 μm width) at 120 $\mu Lmin^{-1}$ while sheath fluid through the inner wall inlet (425 μm width) at a higher flow rate (10×, ~1200 $\mu Lmin^{-1}$) to confine the sample stream near the outer wall (Figure 1B). As the sample traverses the spiral channel, cells from the original sample solution experience F_D and migrate towards the inner wall. Larger cells equilibrate near the inner wall, while the sample solution continues flowing along the Dean vortices and recirculates towards the outer wall.[26] This allows the inertial-focused cells to be replaced with buffer (sheath fluid) and the sample solution (containing unbound particles) to be removed as waste. To achieve complete buffer exchange, the smaller cell outlet (150 μm) proximal to the inner wall is designed to recover the cell suspension, whereas the larger waste outlet (350 μm) ensures the removal of the non-cell fraction.

To determine the optimal flow conditions for complete recirculation of particles and original sample buffer to the channel outer wall, 2 μm beads were used to model Dean migration of the sample solution as the beads are much smaller ($a_p/h \sim 0.017$) and would only be subjected to lateral Dean drag forces in our device. The Stokes number (S_t) for 2 μm particles in our system is ~10^{-5} ($S_t = \tau/t_{rest}$, where $\tau = (\rho_p d_p^2)/(18\mu_f)$ and $t_{rest} \sim 2h^2/\upsilon$. μ_f is fluid viscosity and ρ_p and d_p are particle density and diameter, respectively. h is half channel height and υ is the kinematic viscosity)[32]. Since S_t « 1, it is expected that the particles follow fluid streamlines closely. Bead solution and sheath fluid were pumped into the DFF device at a flow ratio of 1:10 and fluorescence imaging was used to capture their equilibrium position.

As shown in Figure 2A, the 2 μm beads migrated as a tight band under the influence of Dean vortices from the inner wall towards the outer wall as the perfusion speed increased. At a flow rate of 1000 μL/min and above, all the 2 μm beads were collected in the large waste outlet. We then characterized the focusing and equilibrium positions of bead at other sizes (2, 5, 10, and 15 μm) at various flow rate conditions (Figure S1). To ensure efficient removal of free particles while minimizing any shear stress on processed cells, the flow rate was fixed at 1200 μL/min for subsequent experiments. In addition to the flow rate, the specific properties of device design (encompassing channel loops/cycles) are also crucial to maintain maximal separation between 2 and 10 μm beads. Changes to these parameters will compromise this separation distance and reduce efficiency in sorting free nano/microparticles from labelled cells.

Quantifying DFF Microfluidics Separation Efficacy. Next, suspension monocyte cells (THP-1) and 15 μm beads were mixed in a solution containing model biomolecules (food dye (~800Da) or FITC-Dextran, 40kDa) for buffer exchange experiments. These molecules are suitable for demonstrating solution exchange applications as their high Peclet numbers (~1,000-

5,000) indicate negligible diffusive effects[19] (Peclet equation[19]). Their molecular size range also encompasses a broad range of bioimaging and transformative agents payloads (steroids (~500 Da) to proteins (~50-70 kDa)) typically loaded into particles.[5-6] High speed imaging clearly showed that both THP-1 cells and model 15 μm beads were focused and sorted into the cell outlet, while the food dye was directed to the outer region (Figure 2B). To quantify biomolecule depletion, food dye was substituted with FITC-Dextran and nearly all the biomolecules were observed to have been removed, resulting in superior biomolecule depletion efficiency (20 fold) compared to the supernatant obtained from conventional centrifugation (Figure 2C). Moreover, DFF microfluidics exhibited more efficient purification performance with significantly lower cell loss (4.93%) compared to centrifugation (27.1%). This suggests that DFF purification efficiently removes larger NP/MPs used for cell labeling.

Efficient Purification of Labeled Suspension Cells. THP-1 cells were labeled with either silica (~500 nm) or poly(lactic-co-glycolic acid) (PLGA, ~1 μm) NPs through culture media incubation. The efficacy of DFF purification of engineered suspension cells from free particles (silica and PLGA NPs) was next evaluated. Both particles were fluorescent due to the encapsulation of organic dyes (calcein and calcein AM respectively). The mixture of labeled cells and free particles (silica and PLGA NPs) were subsequently introduced into the spiral DFF separation device. Utilizing high speed imaging, efficient purification of THP-1 cells was observed, whereas fluorescence imaging showed that the bulk of the unbound free silica NPs (containing calcein) was channeled into the waste outlet (Figure 3A). To quantify separation efficiency, flow cytometry was employed to analyze samples from both cell and waste outlets based on their distinct forward and side scatter characteristics (Figure S2A). Compared with the unpurified samples, the cell outlet recovered majority of THP-1 cells (95.1 ± 2.1%) with minimal

silica NPs presence, whereas the waste outlet contained most of the NPs (95.2 ± 1.9%) (Figure 3B). Similarly efficient separation was also observed for THP-1 cells labeled with PLGA NPs (Figure S2B). Furthermore, cell recovery performance remained high (>90%) for both labeling methods when sample concentration was increased by 100-fold to 10^7 cells/mL (Figure S3). This is a key improvement over existing inertial microfluidic cell separation methods which are generally limited to 10^5 cells/mL capacity due to cell-cell interaction and cell overcrowding at equilibrium positions[29]

Removal of unbound particles from labeled cells is not trivial since common laboratory separation techniques cannot easily discriminate the constituents of a suspension solution containing different-sized particles (*i.e.* unbound particles and labeled cells). The separation efficiency between DFF and conventional centrifugation separation was then compared (Figure 3C). Before purification, representative images showed that inlet samples consisted of labeled cells suspended in a mixture of free NPs (silica or PLGA). Following centrifugation, the cell fraction still contained significant quantities of free particles, whereas free particles were barely seen following DFF purification. Fluorescence imaging showed that internalized NPs in the engineered THP-1 cells were well retained during DFF purification (insets). Flow cytometry analysis also revealed that centrifugation could only remove 11.4±1.72 % free silica NPs and 37.7±6.63 % free PLGA NPs (Figure 3D). In contrast, DFF was much more efficient, removing 96.2±1.94 % free silica NPs and 97.8±1.47% free PLGA NPs. This clearly demonstrates DFF superior performance over conventional centrifugation in unbound NP removal, a by-product from cell labeling.

A benefit of removing unbound particles from labeled cells is to minimize the mislabeling of non-target by-stander cells. This was assessed using a Transwell® co-culture assay (8 μm) pores

that selectively allow unbound NPs to pass through, whereas cell-cell NP transfer is prevented. Unlabeled THP-1 cells were seeded in 24-wells before inserting Transwell® membranes to create a double-chambered well with an upper and lower deck. PLGA NP labeled THP-1 cells were then seeded in the upper chamber (Figure 3E). After 6 hours incubation, free PLGA NPs from unpurified samples diffused through the insert membrane and labeled THP-1 cells seeded in the lower chamber. In the group using conventional centrifugation to purify particle-engineered THP-1 cells, significant fluorescence signal was observed in the lower chamber cell population that was unlabeled during experiment commencement. Fluorescence signal from these cells were expressed at ~50% that of control free NP cultures. Excitingly, no detectable fluorescent signal was emitted from these cells if the labeled cells from the upper chamber were purified using DFF, which demonstrated efficient removal of fluorescence contrast agent-loaded NPs.

Efficient Purification of Mesenchymal Stem Cells. We next adapted the microfluidic DFF technology to purify cells with greater therapeutic relevance. Unlike THP-1 cells which are ~15 μm and relatively homogeneous in size, MSCs have a highly heterogeneous distribution, ranging between 16 – 28 μm in diameter.[25, 33] In preclinical studies, they are also a popular candidate to engineered with micro/nano-particles to track their bio-distribution following implantation,[34-36] or to endow augmented therapeutic properties.[37-40] To accommodate high cell recovery of the heterogeneous-sized MSCs, minor modifications were made to the spiral device dimensions and its operating characteristics. Specifically, the channel height was increased from 115 μm to 130 μm to enable inertial focusing of larger MSCs. The ratio between cell and waste outlet channels, key to the efficient collection of partitioned cells and unbound NPs, was determined by assessing particle focusing behavior between 3 different types of beads.

The adapted device was assessed using a mixture of 2, 10 and 45 μm beads. 10 and 45 μm beads represent the minimal and maximal MSC dimensions while 2 μm beads represent unbound particles to be removed as waste. As discussed above (Figs. 2 & 3), inertial focusing in the spiral channel tends to focus larger particles closer to the inner wall. However, 45 μm beads ($a_p/h \sim 0.35$) experienced significant Dean drag forces (Stoke's Drag; $F_D \sim a_p$) which slowed down their migration and prevented migration to the inner wall (Figure 4A). Thus large beads (*i.e.* 10 and 45 μm beads) remained focused closer to the channel center while the smaller 2 μm beads completed a Dean cycle back to the outer wall and could be efficiently channeled into the waste outlet (Figure 4B). To facilitate efficient cell collection, the ratio between cell to waste outlet was modified to 3:2 (300 and 200 μm respectively) opposed to 3:7 (150 and 350 respectively) during THP-1 cell purification.

The modified DFF microfluidic device was next used to purify MSCs. Similar to the above experiments with THP-1 cells, MSCs were labeled with Silica and PLGA NPs. Following trypsin dissociation, the mixture was processed using the DFF spiral device. Figure 4C, a representative image during the purification of the MSC and PLGA NP mixture distinctly showed that labeled MSCs were well separated from unbound particles. Efficient separation of MSCs from the particles can be better seen in the attached video (Supporting Information Video 1). High MSC recovery (~90%) was achieved at the cell outlet and the removal of silica NPs and PLGA NPs into the smaller waste outlet was similarly efficient at 88.5% and 97.8% respectively (Figure 4D).

DFF Microfluidic Purification Restore Endothelial Cell Migration. During THP-1 purification, we showed how the successful removal of free fluorescent particles from labeled cells minimized the mislabeling of non-target bystander cells (Fig. 3, above). In the case of

MSCs, we shifted our focus to demonstrate that free particle removal from engineered cells could reduce undesirable interference with bystander cell function. Another significant difference between THP-1 and MSC purification is that the former are suspension whereas the latter are anchorage-dependent cells. Thus, the bulk of free particles from MSC labeling can be removed by washing/media exchange. In this case, we evaluated if DFF purification further reduced interference resulting from free particles that enter solution during processing (washing, dissociation and collection) of adherent cells into a cell suspension.

Dexamethasone (DEX) is a widely used synthetic glucocorticoid compound. Although having numerous benefits for MSC culture,[41-43] DEX can also interfere with endothelial cell migration, function, angiogenesis, and wound healing.[44-45] MSCs have been proposed as a cell-based carrier to achieve spatiotemporal controlled drug delivery by loading PLGA NPs with DEX (DEX-PLGA-NPs).[37-39, 45] Given its potent anti-inflammatory activity,[46-47] inadvertent introduction of free DEX-PLGA-NPs alongside engineered MSCs may cause off-target effects, disrupting normal endothelial function.[48]

Using the Transwell® co-culture system, human umbilical vein endothelial cells (HUVECs) were grown to confluence in the lower chamber before seeding DEX-PLGA-NP labeled MSCs in the upper chamber. A scratch wound assay was performed on HUVECs just prior to seeding the labeled MSCs.[49] To visualize the migrating cells and DEX-PLGA-NPs, HUVECs were labeled using the carbocyanine dye DiB (blue), whereas DEX-PLGA-NPs were co-loaded with red-shifted DiI (red) dye to visualize their presence. As shown in Figure 5, the extent of HUVEC migration after 24 hours of co-culture with unmodified MSCs was similar to those co-cultured with DFF-purified DEX-PLGA-NP labeled MSCs. In both cases, HUVECs restored the separation distance by 80-85% within 24 hours. Moreover, free DEX-PLGA-NPs (red) were not

visible when HUVECs were co-cultured with DFF-purified labeled MSCs (Figure 5A). On the other hand, both DEX-PLGA-NPs (waste) and unpurified DEX-PLGA-NP labeled MSCs (inlet) attenuated the migration distance of HUVECs to 55-60% (Figure 5B). Significant DEX-PLGA-NPs (red signal) was also observed in the HUVEC samples co-cultured with either the contents of the 'waste' outlet (mainly DEX-PLGA-NPs) or contents of the 'inlet' (unpurified MSCs) (Figure 5A). This suggests that free particles were further released despite the washing/media exchange when adherent MSCs were processed into a cell suspension. The presence of red particles in control and DFF purified cells was not observed. Thus DFF microfluidics efficiently purified labeled cells of free DEX-PLGA-NPs to facilitate normal HUVEC migration.

DFF Microfluidic Purification Restore Endothelial – Leukocyte Cell Adhesion. We sought to investigate if other endothelial cell functions apart from migration are impeded by exposure to the unbound DEX-PLGA-NPs after MSC engineering. Leukocyte adhesion with endothelial cells is another critical function facilitating immune cell first-response to bacterial infections and wound healing.[50] This physiological trait facilitates leukocyte adherence to mount an immune response. Endothelial-leukocyte cell adherence depends on the expression of adhesion molecules (*e.g.* endothelial leukocyte adhesion molecule 1, ELAM-1; intercellular adhesion molecule 1, ICAM-1 *etc.*[51]) which increase expression during exposure to inflammatory factors (*e.g.* TNF-α) for enhanced capture and binding between leukocytes and inflamed endothelial cells. However, misdirected anti-inflammatory DEX from free particles could inhibit endothelial-leukocyte cell adherence.

We next studied if exposure to anti-inflammatory DEX from free NPs had any influence on leukocyte adhesion.[48, 52-53] Moreover, we attempted to identify if DFF purification would ameliorate this interference on bystander endothelial cells, if any. Transwell® assay were used to

co-culture DEX-PLGA-NP engineered MSCs (upper chamber) with the HUVEC monolayer (lower chamber) for 24 hours. Thereafter, HUVECs were treated with Tumor necrosis factor (TNF)-α for 4 hours to stimulate inflammation, which was followed by the addition of MitoTracker® Green labeled THP-1 cells for adhesion. Unattached cells were stringently removed by thorough washing before imaging was performed immediately to determine the quantity of attached THP-1 cells. Acquired fluorescence signal was used to indirectly quantify attached monocytes.

As seen in Figure 6B, TNF-α treatment increased THP-1 adhesion on the HUVEC monolayer adjudged by the ~45 fold increase in fluorescence emission presumably through up-regulated adhesion moieties.[54] However, when THP-1 cells were introduced after exposure to DEX-PLGA-NPs ('waste' outlet), the fluorescence signal decreased by ~40%. Similar attenuation was observed when THP-1 cells were introduced to TNF-α treated HUVECs together with unpurified MSCs. However, when DFF purification was performed to remove unbound DEX-PLGA-NPs, the THP-1 cells retained adhesion with HUVECs. These demonstrate how unbound anti-inflammatory DEX-PLGA-NPs attenuate TNF-α stimulation of HUVECs and subsequently reduce THP-1 cell adhesion which signifies interference with normal HUVEC behavior. On the other hand, efficient removal of unbound DEX-PLGA-NPs using DFF purification removes interference and restores leukocyte-endothelial cell adhesion, a critical immune cell response.

CONCLUSIONS

Engineering cells with micro/nano-particles is becoming a widely used, facile and versatile method to enable cell tracking as well as augment native cell therapeutic properties. However, we reveal critical concerns regarding the unintentional transfer of imaging signal (PLGA-CAM) and transformative agents (DEX) onto bystander non-target cells. The remnant NPs that remain

following cell labeling, cannot be readily separated using conventional centrifugation. To address this issue, a novel cell purification strategy using inertial microfluidics in spiral microchannel (DFF) was applied to efficiently remove unbound particles from labeled cells in a rapid, safe and continuous manner. Unlike other inertial microfluidics-based buffer exchange strategies[19-21], the developed DFF technique was able to exchange buffer solution from target cells with ultra-high efficiency (>99.9%) due to the large channel width (500 μm) for buffer and small particles to migrate further away from the labeled cells prior separation.

The DFF microfluidic device operates at ultra-high cell throughput ($\leq 10^6$ cells/min) and has the requisite resolution and versatility to separate cells of differing dimensions merely through the minor adjustment of device geometry and operating conditions. This was evident during the transition from purifying homogeneous-sized monocytes to heterogeneous-sized MSCs. Furthermore, the process is scalable, since cell concentration can be increased 100-fold without compromising performance (Figure S3). We show that the inadvertent transfer of unbound particles to bystander non-target cells is an undesirable trait that occurs as a result of cell labeling. Using DFF microfluidic purification, unbound fluorescent particles (Silica and PLGA NPs) could be removed from monocytic suspension cells (THP-1), eliminating fluorescence signal transferred to unlabeled cells. Unbound particles loaded with transformative agents (e.g. DEX) also risk generating off-target effects. We showed that unpurified engineered MSCs containing unbound DEX-PLGA-NPs attenuate physiological (migration assay) and pathological (leukocyte adhesion assay) responses in endothelial cells. Yet, these properties were restored following DFF purification of DEX-PLGA-NP engineered MSCs.

Given that DFF microfluidics utilizes fluid mechanics (fluid flow and spiral design properties) as a basis for particle separation, it is unequipped to sort cells based on the expression of

particular cellular properties. These could include cell surface markers, viability, or any other cell biomarkers. The inclusion of other sorting mechanisms that utilize 'active' separation techniques such as magnetic, acoustic forces and optical signals in combination with biomolecule recognition (e.g. antibodies, aptamers) can facilitate higher resolution separation of a given target cell population. While diminished cell viability due to shear stress from DFF is a possible source for concern, this is likely to be an unfounded concern due to the short residence time (<1 sec) within the microfluidic channel. Previous studies using similar DFF separation devices also demonstrated no differences between cell viability for sorted and unsorted cells.[55]

In summary, conventional centrifugation has limited efficacy in removing unbound particles during the cell engineering with micro/nano-particles. Besides giving rise to false positive imaging contrast, free drug-loaded particles also become inadvertently transferred to non-target cells. DFF microfluidic technology offers an elegant and efficient solution to remove unbound micro/nano-particles in a continuous manner. Its successful implementation allows the interference-free usage of particle-based cell engineering for therapy.

MATERIALS AND METHODS

Cell Culture. THP-1 cells (ATCC), a human monocytic cell line, was cultured in Roswell Park Memorial Institute (RPMI) 1640 medium (Lonza) supplemented with 10 % fetal bovine serum (FBS) (Gibco®) and 0.05 mM 2-mercaptoethanol (Sigma). Human umbilical vein endothelial cells (HUVEC) (Lonza) were cultured in endothelial cell growth medium (EGM) (Lonza) supplemented with 10% FBS. Meanwhile, Mesenchymal Stem Cells (MSC) (Lonza) were cultured in Dulbecco's Modified Eagle's medium (DMEM) (Lonza) supplemented with 10% FBS. They were all maintained at 37 ºC, a humidified 5% CO_2 atmosphere and were fed thrice weekly.

Nanoparticle Fabrication. Silica NPs (~500 μm, Sigma) were purchased from Sigma and loaded with calcein dye through overnight stirring (500 rpm) in concentrated calcein solution (200 μM). PLGA particles (*i.e.* CAM-PLGA, DEX-PLGA, and DEX/DiI-PLGA) were synthesized using a single emulsion procedure.[35] Initially, solutions containing either 250 μg CAM, 10 mg DEX or 10 mg DEX with 20 ul DiI (100 μM) in 2 ml chloroform was mixed with 100 mg PLGA (50:50) at 4 ºC. Each mixture was then added drop-wise to 3% (w/v) polyvinyl alcohol (PVA) aqueous solution before homogenization (Tissue Master 125, Omni International) at 24,000 rpm for 60 s. The emulsion was placed in the chemical hood for at least 3 hours to allow chloroform evaporation. Finally, NPs were collected through centrifugation at 6,000 rpm for 5 minutes and washed thrice with double-distilled water before freezing-drying (-80 ºC). Lyophilization was performed to prolong NP storage and samples were stored in -20ºC until just prior to usage.

Cell labeling with particles. Cells were seeded 24 hours before at ≥80% confluency. Prior to cell labeling, CAM-PLGA-NP (1 mg), Silica-NP (150 μg), DEX-PLGA (0.1 mg) and DEX/DiI-PLGA (0.1 mg) were incubated in poly-L-Lysine (PLL) 0.01% solution (Sigma) at room temperature for 15-20 mins. After centrifugation and removal of excess PLL supernatant, NPs were resuspended in 1 ml culture medium and incubated together with cells for approximately 24 hours (0.1 mg/mL labeling concentration). Finally, the labeled cells were dissociated using trypsin (5 minutes, 37 ºC) and collected for subsequent analysis.

Device Fabrication. The spiral microfluidic devices were fabricated based on standard soft lithography methods using polydimethylsiloxane (PDMS).[26] Briefly, PDMS prepolymer was mixed with curing agent in a 10:1 ratio and silicon wafer patterned with channel design was used as template for replica molding. The PDMS mixture was cured after baking at 80° C for 2 hours

and peeled from the master. 1.5 mm holes were punched for the inlets and outlets of the microchannels and the PDMS device was subsequently bonded to a 1 mm thick glass slide using an air plasma machine (Harrick Plasma Cleaner).

Device Characterization. Fluorescent polystyrene beads (~10^{5-6}/mL) of defined sizes (2 μm, 5 μm, 10 μm and 15 μm) were tested at different flow rates (1000, 1200, 1300 and 1400 μL/min) and imaged using fluorescence microscopy. During operation, sample and sheath buffer containing PBS with 0.1% bovine serum albumin (BSA) were injected into the channel inlets at a flow ratio of 1:10 using separate syringe pumps (Chemyx Inc, USA). An inverted phase contrast microscope (Nikon Eclipse Ti) with Metamorph software (Molecular Devices, USA) was used to capture equilibrium positions of different bead sizes during flow. Once flow rate conditions were optimized, mixtures of labeled cells with free particles were similarly injected into the device for separation and phase contrast bright field videos were captured using a high speed camera (Phantom V9.1, USA).

Flow Cytomery. Eluents from both cell and waste outlets were collected and compared with inlet sample (~10^6 labeled cells/mL) using flow cytometry (N≥4, with > 10,000 events taken into account). For centrifuge comparison, the same cell samples were separately purified using conventional benchtop centrifugation (operated at 350g). BD LSR Fortessa flow cytometer (BD Biosciences, USA) was used to analyze the recovery and removal efficiency of labeled cells and free particles, respectively.

Quantifying Biomolecule Depletion. To determine buffer exchange efficiency, FITC-Dextran (40kDa) solution (10 mg/mL) (Sigma-Aldrich) was processed using the spiral device. Eluents from the cell outlet and waste outlet were collected and analyzed using microplate reader (BioTek). A standard fluorescence curve using pre-defined concentrations of FITC-Dextran 40

was obtained and biomolecule depletion factor was calculated based on fluorescence signal of cell outlet/inlet sample. For high speed imaging, food dye (Apple green, M_W= 800Da, 1:100) was used as a means to visualize its lateral migration within the microchannel during DFF processing.

Transwell Assays. The experiments were typically performed by introducing a given condition of cells (*e.g*. unmodified sample, DFF purified, centrifuge purified *etc*.) into the upper compartment to assess its effect on unlabeled cells (THP-1, HUVECs) in the lower compartment.

(a) CAM-PLGA-NP Labeling Transwell® Assay

To evaluate the usage of this device to prevent fluorescent particle transfer, THP-1 cells (~10^6 cells/ml) labeled with CAM-PLGA-NP (1 mg/mL) were seeded on 8 μm pore transwells (Corning®) that overlaid a layer of unlabeled THP-1 cells (~10^6 cells/mL), prior to and after centrifugation as well as DFF free particle purification. 6 hours post seeding, fluorescence images were obtained using LX71 inverted fluorescent microscope (Olympus) and quantified for average cell fluorescent intensity by ImageJ software (n≥200 cells).

(b) Migration Transwell® Assay

DEX/DiI-PLGA-NP (1 mg/mL) labeled MSCs (~10^6 cells) were introduced to the Transwell® assays with or without prior DFF purification. Prior to experimental commencement, a confluent layer of HUVECs below was scratched with 200μl pipette tips along the entire length of a 24-well plate well to simulate a 'wound' to facilitate HUVEC migration response.[49] The widths of the wounded area were measured after 12 & 24 hours, and normalized against the initial width to obtain the migration distances of the HUVECs (ImageJ). Additionally, the HUVECs on the bottom layer were stained with 4 μM DIB for 10-15 minutes to facilitate cellular boundary identification during fluorescent imaging.

(c) Monocyte Adhesion Transwell® Assay

Transwell® inserts were placed on the top of a confluent layer of HUVECs. Each assay (24-well and insert) was seeded with dissociated DEX-PLGA-NP engineered MSCs (~10^6 cells) with and without DFF purification for 24 hours. Transwell® inserts were removed and HUVECs were treated with TNF-α (10 ng/mL in EGM) for 4 hours to induce inflammation. THP-1 monocytes were labeled with MitoTracker Green® FM (100 nM, Invitrogen) at 37ºC for 30 minutes. Labeled THP-1 cells were then incubated at a density of 2×10^5 cells per well (500 μL EGM) for an hour and imaged after thorough washing with PBS to remove any non-adherent cells. Fluorescence images were captured at 10 and 20x magnifications using a fluorescent microscope and fluorescence signal intensity (indicative of THP-1 adherence) quantified using ImageJ software.

Supporting Information Available: Details regarding optimization of microfluidic device flow rates for particles of different sizes, flow cytometry gating of unbound particles (Silica and PLGA) and cells using their forward and side scatter characteristics and separation efficiency of particles from cells at higher cell concentration levels ($10^{5\text{-}7}$ cells/mL). A short video showing the efficient separation of MSCs from PLGA microparticles is also included. This material is available free of charge *via* the Internet at http://pubs.acs.org.

Corresponding Author

*Address correspondence to H.W.H. (hwhou@ntu.edu.sg), C.J.X. (cjxu@ntu.edu.sg).

Conflict of Interest

The authors declare no competing financial interest.

Author Contributions

The manuscript was written through contributions of all authors. All authors have given approval to the final version of the manuscript. Specifically, D.Y., H.W.H., and C.J.X. conceived the project and wrote the manuscript. D.Y., C.W., Y. Z., H.M.T and H.W.H. performed the experiments. H.W.H. prepared the figures.

Funding Sources

This project is funded by NTU-Northwestern Institute of Nanomedicine (Nanyang Technological University). H.W.H. is supported by Lee Kong Chian School of Medicine (LKC-Medicine, Singapore) Postdoctoral Fellowship.

ACKNOWLEDGMENT

The authors acknowledge the kind gift of THP-1 cells and HUVECs from Dr. Mark Chong and assistance in microfabrication from Dr. Yuejun Kang and Nishanth V. Menon (School of Chemical and Biomedical Engineering, Nanyang Technological University).

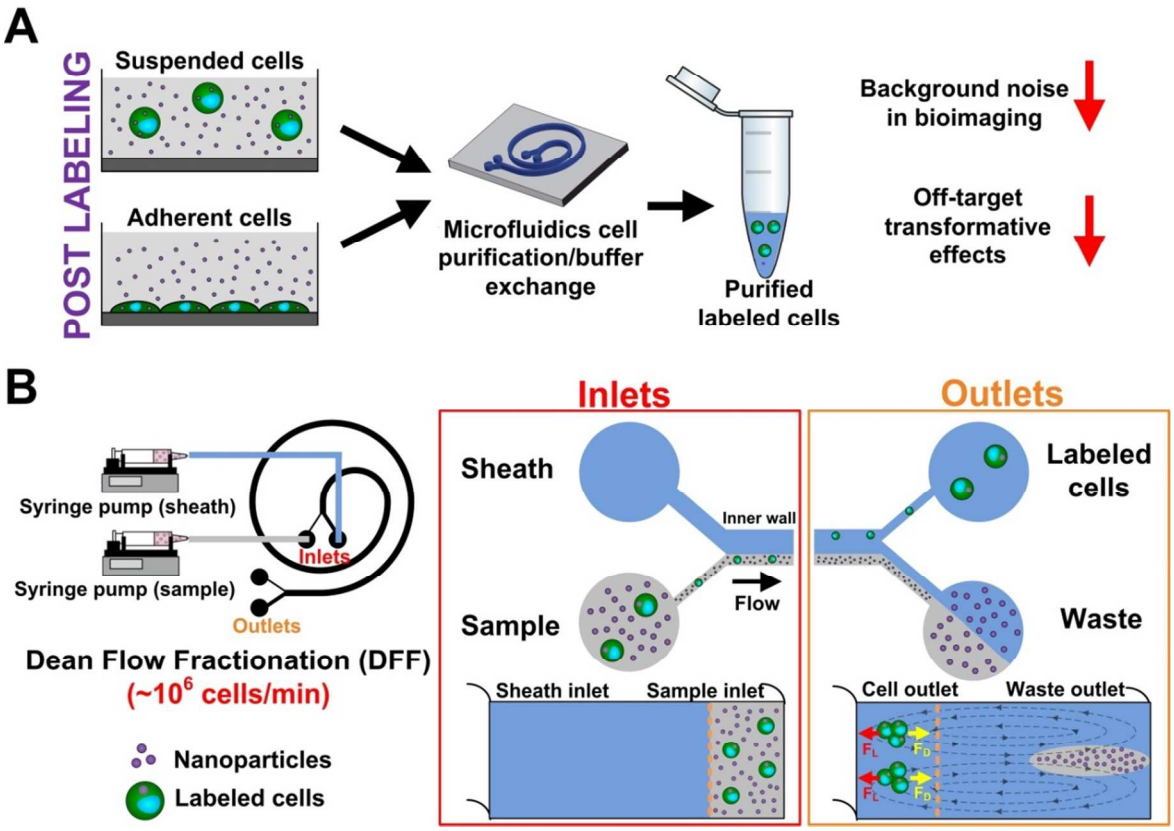

Figure 1. Application of Dean Flow Fractionation (DFF) for buffer exchange and nanoparticles removal in particle based cell engineering. (A) Overall workflow for single-step NPs removal from suspended and adherent cells post-labeling. Purified labeled cells have reduced bioimaging and off-target interference. (B) Schematic illustration of the DFF in spiral device. Setup utilizes syringe pumps for continuous perfusion of labeled cells at high throughput (~10^{5-7}/mL). Under the influence of Dean drag forces (F_D (yellow arrows), labeled cells in NPs-containing buffer solution migrate from the outer wall towards inner wall. Larger cells experience additional strong inertial lift forces (F_L (red arrows)) and focus near the micro-channel inner wall while NPs and buffer solution recirculates to the outer wall. This facilitates the collection of labeled cells in buffer solution through the cell outlet, while NPs and other non-cell constituents are collected in the waste channel. Dotted lines (orange) indicate bifurcation positions between 2 inlets and outlets.

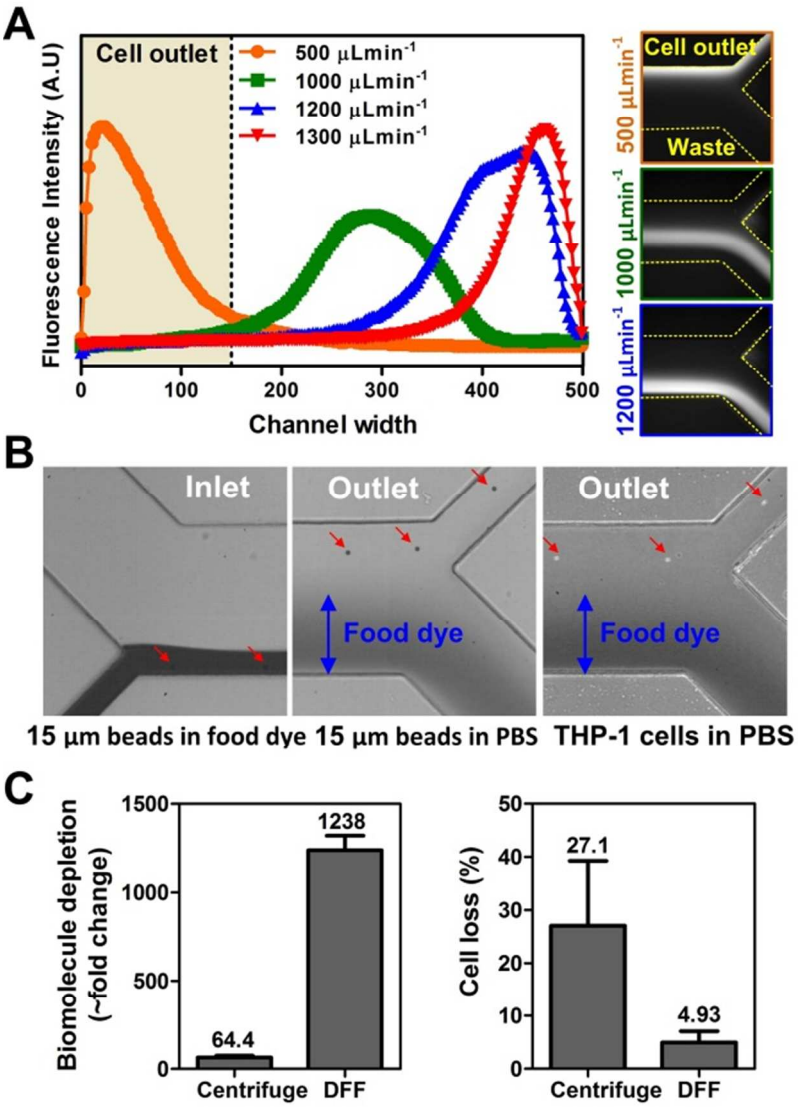

Figure 2. Buffer exchange using DFF. (A) Average fluorescence intensity line scans show the distribution of 2 μm beads across the channel width at increasing flow rates. Approximate position of the cell outlet (150 μm wide) at inner wall (origin) is indicated. Corresponding fluorescence images illustrate flow positions of 2 μm beads at different flow rates are also shown (yellow dashed lines indicate the approximate position of the microchannel walls). (B) High speed images at the inlet and outlet show efficient buffer exchange of representative biomolecule (food dye) solution with 15 μm beads and THP-1 cells. Food dye (dark colored, blue arrows) are recirculated to the outer wall and removed as waste while inertial-focused beads and cells (red

arrows) are replaced with sheath buffer and focused into the cell outlet. (C) Superior buffer exchange performance of DFF technology based on ~20-fold increase in biomolecule depletion with lower cell loss (~4.93%) compared to centrifugation. Values are N=3, mean ± SD.

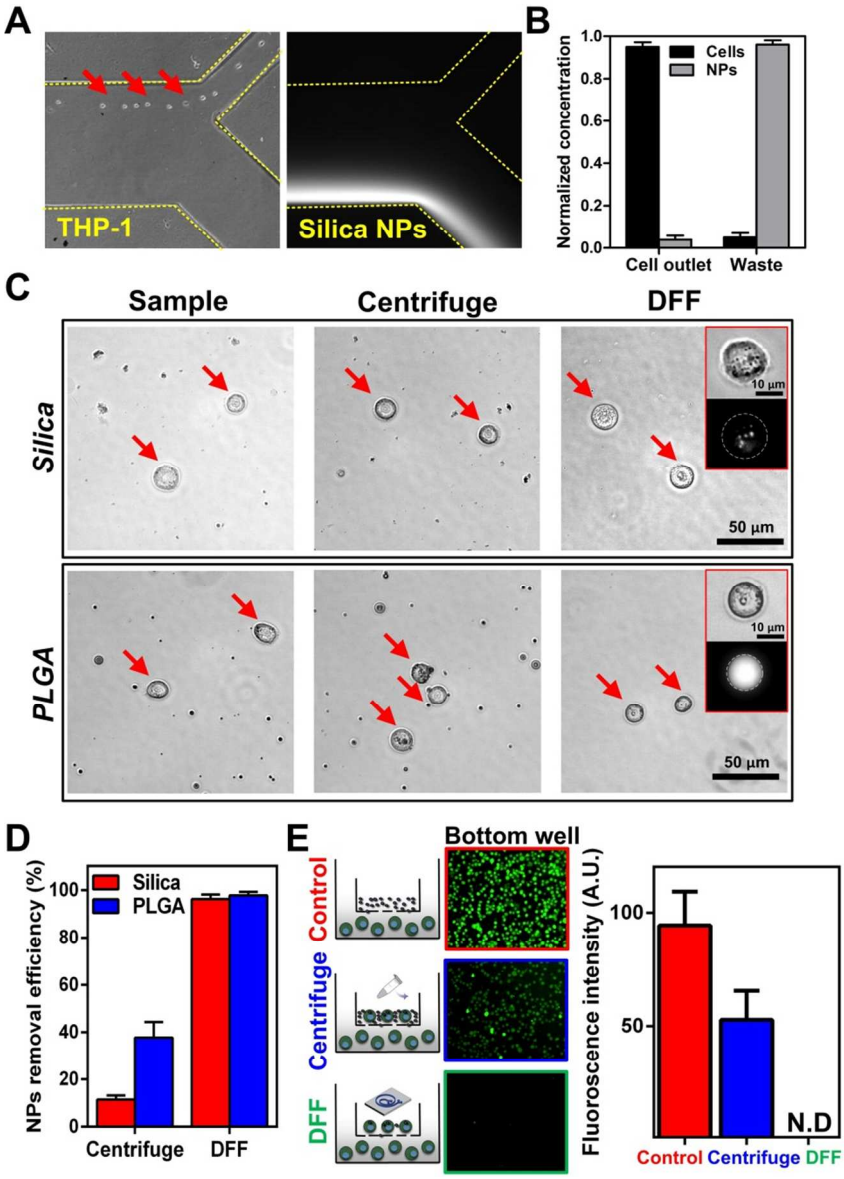

Figure 3. Nanoparticles (NPs) removal from THP-1 cells using DFF. (A) High speed and fluorescence images indicating distinct equilibrium positions of THP-1 cells (red arrows) and silica NPs loaded with calcein dye. Yellow dashed lines indicate the approximate position of the microchannel walls. (B) Separation performance of cells and silica NPs based on flow cytometry

analysis. (C) Representative bright field images of purified labeled THP-1 cells (red arrows) and (D) NPs removal efficiency using centrifuge and DFF. (E) Non detectable fluorescence signal in unlabeled THP-1 cells at bottom well after 24 hours co-culture with DFF-purified labeled THP-1 (upper chamber) using Transwell assay (8.0 µm pores). In contrast, high fluorescence signals were detected in control (NPs only) and centrifuge-purified THP-1 cells. Values are N=3, mean ± SD.

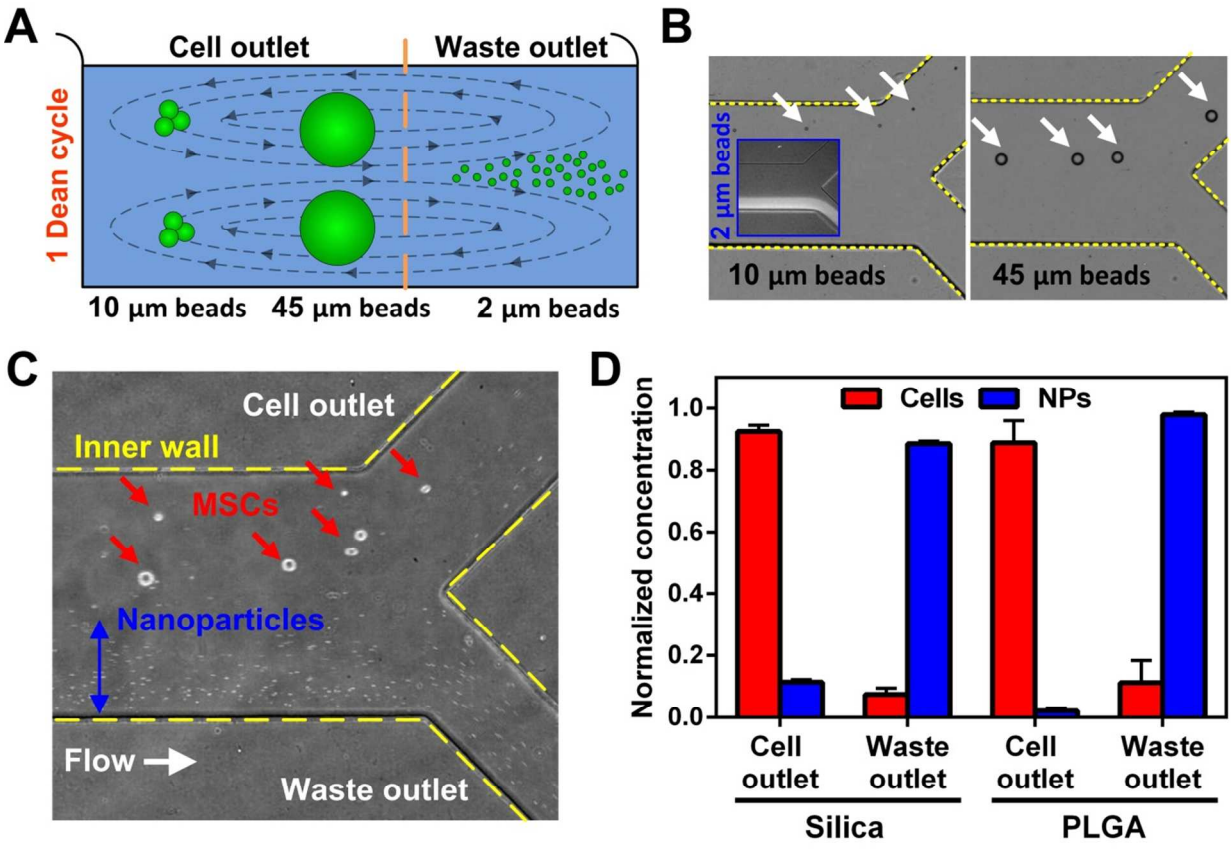

Figure 4. Unbound nanoparticle removal from mesenchymal stem cells (MSCs) using DFF. (**A**) Schematic of channel cross section indicating the approximate equilibrium position of different-sized beads. At optimized flow conditions, 10 µm beads are inertial-focused at the inner wall while the 45 µm beads remain closer to the channel centre as they experience significant Stoke's Drag which impairs their migration to the inner wall. 2µm beads (and consequently NPs)

complete a recirculation back to the outer wall. (**B**) High speed images confirm flow positions of 10 and 45 μm beads (white arrows). Inset fluorescence image (blue box) indicates the flow position of 2μm beads at the same flow rate. (**C**) Representative high speed image illustrating efficient separation of MSCs (red arrows) and PLGA NPs (blue arrows) into different outlets. Yellow dashed lines indicate the approximate position of the microchannel walls. (**D**) Separation performance of MSCs from silica and PLGA NPs. Values are N=3, mean ± SD.

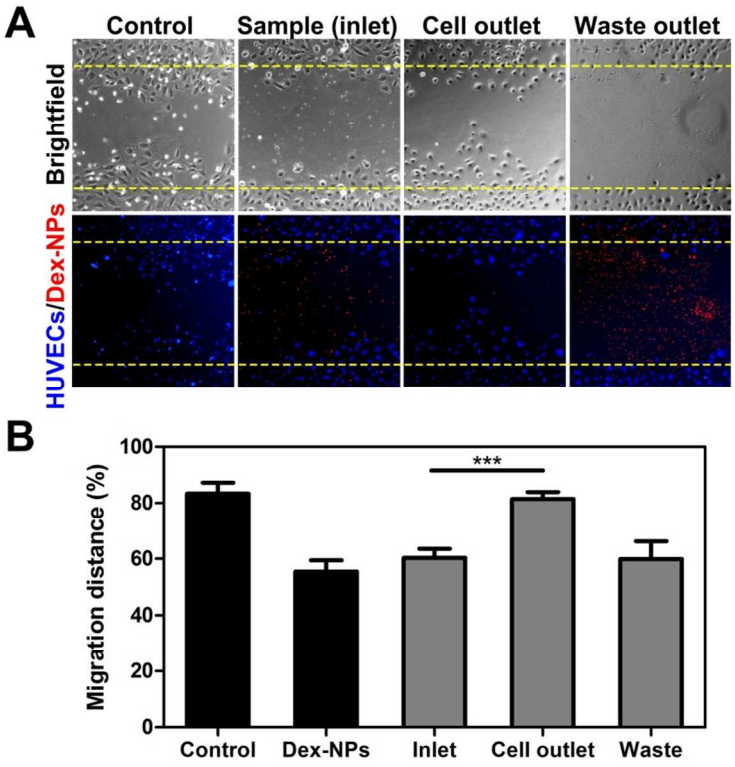

Figure 5. HUVEC migration assay after co-culture with mesenchymal stem cells (MSCs) labeled with dexamethasone loaded particles (DEX-NPs). (**A**) Representative phase contrast and fluorescence images of HUVEC migration after 24 hours when co-cultured with MSCs from control, inlet (before purification) and DFF-sorted (after purification) samples. Yellow dotted lines represent the original separation following the inflicted 'wound' on the confluent cell monolayer at Time=0. Cells are stained blue with DiB and DEX-NPs red with DiI (**B**)

Normalized migration distance at different conditions. A significant increase in migration distance was observed in HUVECs when co-cultured with DFF-purified MSCs from cell outlet as compared to inlet MSCs (containing free DEX-NPs). Values are N=3, mean ± SD. ***P < 0.001.

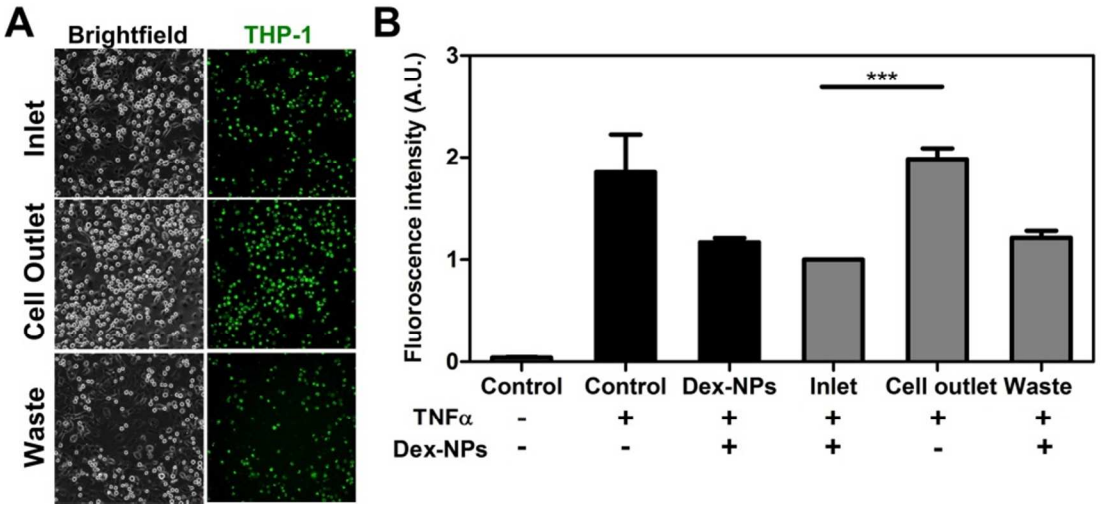

Figure 6. THP-1 adhesion assay after co-culture with mesenchymal stem cells (MSCs) labeled with dexamethasone loaded particles (DEX-NPs). (**A**) Representative bright-field and fluorescence images of TNFα-treated HUVECs monolayer illustrating adhesion of THP-1 cells (stained with MitoGreen®). (**B**) Normalized fluorescence signal indicating THP-1 cells adhesion to HUVECs monolayer when co-cultured with MSCs from controls, inlet (before purification) and DFF-sorted (after purification) samples. A significant increase in THP-1 adhesion on HUVECs was observed when co-cultured with DFF-purified MSCs from cell outlet as compared to inlet MSCs (containing free DEX-NPs). Values are N=3, mean ± SD. ***P < 0.001.

REFERENCES

1. Wiraja, C.; Yeo, D.; Lio, D.; Labanieh, L.; Lu, M.; Zhao, W.; Xu, C. Aptamer Technology for Tracking Cells' Status & Function. *Mol. Cell. Ther.* **2014,** 2, 33.

.2. Yeo, D. C.; Wiraja, C.; Mantalaris, A.; Xu, C. Nanosensors for Regenerative Medicine. *J. Biomed. Nanotech.* **2014**, 10, 2722-2746.

3. Naumova, A. V.; Modo, M.; Moore, A.; Murry, C. E.; Frank, J. A. Clinical Imaging in Regenerative Medicine. *Nat. Biotechnol.* **2014**, *32*, 804-818.

4. de Vries, I. J.; Lesterhuis, W. J.; Barentsz, J. O.; Verdijk, P.; van Krieken, J. H.; Boerman, O. C.; Oyen, W. J.; Bonenkamp, J. J.; Boezeman, J. B.; Adema, G. J.; Bulte, J. W.; Scheenen, T. W.; Punt, C. J.; Heerschap, A.; Figdor, C. G. Magnetic Resonance Tracking of Dendritic Cells in Melanoma Patients for Monitoring of Cellular Therapy. *Nat. Biotechnol.* **2005**, 23, 1407-1413.

5. Cristiana, S. O. P.; Ricardo Pires das, N.; Lino, S. F. Nanoparticles for Intracellular-Targeted Drug Delivery. *Nanotechnology* **2011**, 22, 494002.

6. Stuckey, D. W.; Shah, K. Stem Cell-Based Therapies for Cancer Treatment: Separating Hope from Hype. *Nat. Rev. Cancer* **2014**, 14*,* 683-691.

7. Karp, J.; Zhao, W. *Micro-and Nanoengineering of the Cell Surface*, 1st Ed; William Andrew Publisher: Oxford, 2014.

8. Soenen, S. J.; Rivera-Gil, P.; Montenegro, J.-M.; Parak, W. J.; De Smedt, S. C.; Braeckmans, K. Cellular Toxicity of Inorganic Nanoparticles: Common Aspects and Guidelines for Improved Nanotoxicity Evaluation. *Nano Today* **2011**, 6, 446-465.

9. Donaldson, K.; Poland, C. A. Nanotoxicity: Challenging the Myth of Nano-Specific Toxicity. *Curr. Opin. Biotechnol.* **2013**, 24, 724-734.

10. Gale, J. S.; Proulx, A. A.; Gonder, J. R.; Mao, A. J.; Hutnik, C. M. L. Comparison of the In Vitro Toxicity of Indocyanine Green to that of Trypan Blue in Human Retinal Pigment Epithelium Cell Cultures. *Am. J. Ophthalmol.* **2004**, 138, 64-69.

11. Veiseh, O.; Doloff, J. C.; Ma, M.; Vegas, A. J.; Tam, H. H.; Bader, A. R.; Li, J.; Langan, E.; Wyckoff, J.; Loo, W. S.; Jhunjhunwala, S.; Chiu, A.; Siebert, S.; Tang, K.; Hollister-Lock, J.; Aresta-Dasilva, S.; Bochenek, M.; Mendoza-Elias, J.; Wang, Y.; Qi, M.; Lavin, D. M.; Chen, M.; Dholakia, N.; Thakrar, R.; Lacik, I.; Weir, G. C.; Oberholzer, J.; Greiner, D. L.; Langer, R.; Anderson, D. G. Size- and Shape-Dependent Foreign Body Immune Response to Materials Implanted in Rodents and Non-Human Primates. *Nat. Mater.* **2015,** 14, 643-651.

12. Moghimi, S. M.; Hunter, A. C.; Andresen, T. L. Factors Controlling Nanoparticle Pharmacokinetics: An Integrated Analysis and Perspective. *Annu. Rev. Pharmacol. Toxicol.* **2012**, 52, 481-503.

13. Jones, S. W.; Roberts, R. A.; Robbins, G. R.; Perry, J. L.; Kai, M. P.; Chen, K.; Bo, T.; Napier, M. E.; Ting, J. P. Y.; DeSimone, J. M.; Bear, J. E. Nanoparticle Clearance is Governed by Th1/Th2 Immunity and Strain Background. *J. Clin. Invest.* **2013**, 123, 3061-3073.

14. Marchi, L.; Sesti-Costa, R.; Chedraoui-Silva, S.; Mantovani, B. Comparison of Four Methods for the Isolation of Murine Blood Neutrophils with Respect to the Release of Reactive Oxygen and Nitrogen Species and the Expression of Immunological Receptors. *Comp. Clin. Pathol.* **2014**, 23, 1469-1476.

15. Morton, K. J.; Loutherback, K.; Inglis, D. W.; Tsui, O. K.; Sturm, J. C.; Chou, S. Y.; Austin, R. H. Hydrodynamic Metamaterials: Microfabricated Arrays to Steer, Refract, and Focus Streams of Biomaterials. *Proc. Natl. Acad. Sci.U. S. A.* **2008**, 105, 7434-7438.

16. Hu, X.; Bessette, P. H.; Qian, J.; Meinhart, C. D.; Daugherty, P. S.; Soh, H. T. Marker-Specific Sorting of Rare Cells Using Dielectrophoresis. *Proc. Natl. Acad. Sci. U. S. A.* **2005**, 102, 15757-15761.

17. Cummings, E. B. Streaming Dielectrophoresis for Continuous-Flow Microfluidic Devices. *IEEE Eng. Med. Biol. Mag.* **2003**, 22, 75-84.

18. Augustsson, P.; Persson, J.; Ekstrom, S.; Ohlin, M.; Laurell, T. Decomplexing Biofluids Using Microchip Based Acoustophoresis. *Lab Chip* **2009**, 9, 810-818.

19. Gossett, D. R.; Tse, H. T. K.; Dudani, J. S.; Goda, K.; Woods, T. A.; Graves, S. W.; Di Carlo, D. Inertial Manipulation and Transfer of Microparticles Across Laminar Fluid Streams. *Small* **2012**, 8, 2757-2764.

20. Amini, H.; Sollier, E.; Masaeli, M.; Xie, Y.; Ganapathysubramanian, B.; Stone, H. A.; Di Carlo, D. Engineering Fluid Flow using Sequenced Microstructures. *Nat. Commun.* **2013**, 4, 1826.

21. Sollier, E.; Amini, H.; Go, D.; Sandoz, P.; Owsley, K.; Di Carlo, D. Inertial Microfluidic Programming of Microparticle-Laden Flows for Solution Transfer around Cells and Particles. *Microfluid. Nanofluid.* **2015**, 1-13.

22. Hur, S. C.; Henderson-MacLennan, N. K.; McCabe, E. R. B.; Di Carlo, D. Deformability-based Cell Classification and Enrichment using Inertial Microfluidics. *Lab Chip* **2011**, 11, 912-920.

23. Mach, A. J.; Di Carlo, D. Continuous Scalable Blood Filtration Device Using Inertial Microfluidics. *Biotechnol. Bioeng.* **2010**, 107, 302-311.

24. Di Carlo, D.; Irimia, D.; Tompkins, R. G.; Toner, M. Continuous Inertial Focusing, Ordering, and Separation of Particles in Microchannels. *Proc. Natl. Acad. Sci. U. S. A.* **2007**, 104, 18892-18897.

25. Lee, W. C.; Shi, H.; Poon, Z.; Nyan, L. M.; Kaushik, T.; Shivashankar, G. V.; Chan, J. K. Y.; Lim, C. T.; Han, J.; Van Vliet, K. J. Multivariate Biophysical Markers Predictive of Mesenchymal Stromal Cell Multipotency. *Proc. Natl. Acad. Sci.U.S.A.* **2014**, 111, E4409-E4418.

26. Hou, H. W.; Warkiani, M. E.; Khoo, B. L.; Li, Z. R.; Soo, R. A.; Tan, D. S.-W.; Lim, W.-T.; Han, J.; Bhagat, A. A. S.; Lim, C. T. Isolation and Retrieval of Circulating Tumor Cells using Centrifugal Forces. *Sci. Rep.* **2013**, 3, 1259

27. Dean, W. The Stream-line Motion of Fluid in a Curved Pipe. *Philos. Mag. Series 7* **1928**, 5, 673-695.

28. Bhagat, A. A. S.; Kuntaegowdanahalli, S. S.; Papautsky, I. Continuous Particle Separation in Spiral Microchannels using Dean Flows and Differential Migration. *Lab Chip* **2008**, 8, 1906-1914.

29. Kuntaegowdanahalli, S. S.; Bhagat, A. A. S.; Kumar, G.; Papautsky, I. Inertial Microfluidics for Continuous Particle Separation in Spiral Microchannels. *Lab Chip* **2009**, 9, 2973-2980.

30. Wu, L.; Guan, G.; Hou, H. W.; Bhagat, A. A. S.; Han, J. Separation of Leukocytes from Blood Using Spiral Channel with Trapezoid Cross-Section. *Anal. Chem.* **2012**, 84, 9324-9331.

31. Martel, J. M.; Toner, M. Particle Focusing in Curved Microfluidic Channels. *Sci. Rep.* **2013**, 3, 3340.

32. Winer, M. H.; Ahmadi, A.; Cheung, K. C. In *Effects of Density Difference Between Particles and Fluid on Inertial Focusing Positions in Transient Microflows*, 18th International Conference on Miniaturized Systems for Chemistry and Life Sciences, San Antonio, San Antonio, **2014**; 2462-2464.

33. Caplan, A. I., Adult Mesenchymal Stem cells for Tissue Engineering Versus Regenerative Medicine. *J. Cell. Physiol.* **2007**, *213*, 341-347.

34. Gao, Y.; Wang, Y.; Fu, A.; Shi, W.; Yeo, D.; Luo, K. Q.; Ow, H.; Xu, C., Tracking Mesenchymal Stem Cell Tumor-Homing using Fluorescent Silica Nanoparticles. *J. Mater. Chem B* **2015**, *3*, 1245-1253.

35. Xu, C.; Miranda-Nieves, D.; Ankrum, J. A.; Matthiesen, M. E.; Phillips, J. A.; Roes, I.; Wojtkiewicz, G. R.; Juneja, V.; Kultima, J. R.; Zhao, W.; Vemula, P. K.; Lin, C. P.; Nahrendorf, M.; Karp, J. M. Tracking Mesenchymal Stem Cells with Iron Oxide Nanoparticle Loaded Poly(lactide-co-glycolide) Microparticles. *Nano Lett.* **2012**, 12, 4131-4139.

36. Jokerst, J. V.; Khademi, C.; Gambhir, S. S. Intracellular Aggregation of Multimodal Silica Nanoparticles for Ultrasound-Guided Stem Cell Implantation. *Sci. Transl. Med.* **2013**, 5, 177ra35.

37. Ankrum, J. A.; Dastidar, R. G.; Ong, J. F.; Levy, O.; Karp, J. M. Performance-Enhanced Mesenchymal Stem Cells via Intracellular Delivery of Steroids. *Sci. Rep.* **2014**, 4, 4645.

38. Sarkar, D.; Ankrum, J. A.; Teo, G. S.; Carman, C. V.; Karp, J. M., Cellular and Extracellular Programming of Cell Fate Through Engineered Intracrine-, Paracrine-, and Endocrine-like Mechanisms. *Biomaterials* **2011**, 32, 3053-3061.

39. Bernardino, L.; Eiriz, M. F.; Santos, T.; Xapelli, S.; Grade, S.; Rosa, A. I.; Cortes, L.; Ferreira, R.; Bragança, J.; Agasse, F.; Ferreira, L.; Malva, J. O. Histamine Stimulates Neurogenesis in the Rodent Subventricular Zone. *Stem Cells* **2012**, 30, 773-784.

40. Li, L.; Tang, F.; Liu, H.; Liu, T.; Hao, N.; Chen, D.; Teng, X.; He, J. In Vivo Delivery of Silica Nanorattle Encapsulated Docetaxel for Liver Cancer Therapy with Low Toxicity and High Efficacy. *ACS Nano* **2010**, 4, 6874-6882.

41. Song, I.-H.; Caplan, A. I.; Dennis, J. E. Dexamethasone Inhibition of Confluence-Induced Apoptosis in Human Mesenchymal Stem Cells. *J. Orthop. Res.* **2009**, 27, 216-221.

42. Xiao, Y.; Peperzak, V.; van Rijn, L.; Borst, J.; de Bruijn, J. D. Dexamethasone Treatment during the Expansion Phase Maintains Stemness of Bone Marrow Mesenchymal Stem Cells. *J. Tissue Eng. Regen. Med.* **2010**, 4, 374-386.

43. Koehler, K. C.; Alge, D. L.; Anseth, K. S.; Bowman, C. N. A Diels–Alder Modulated Approach to Control and Sustain the Release of Dexamethasone and Induce Osteogenic Differentiation of Human Mesenchymal Stem Cells. *Biomaterials* **2013**, 34, 4150-4158.

44. Logie, J. J.; Ali, S.; Marshall, K. M.; Heck, M. M. S.; Walker, B. R.; Hadoke, P. W. F., Glucocorticoid-Mediated Inhibition of Angiogenic Changes in Human Endothelial Cells Is Not Caused by Reductions in Cell Proliferation or Migration. *PLoS ONE* **2010**, 5, e14476.

45. Shikatani, E. A.; Trifonova, A.; Mandel, E. R.; Liu, S. T.; Roudier, E.; Krylova, A.; Szigiato, A.; Beaudry, J.; Riddell, M. C.; Haas, T. L. Inhibition of Proliferation, Migration and Proteolysis Contribute to Corticosterone-Mediated Inhibition of Angiogenesis. *PLoS ONE* **2012**, 7, e46625.

46. Hickey, T.; Kreutzer, D.; Burgess, D. J.; Moussy, F. Dexamethasone/PLGA Microspheres for Continuous Delivery of an Anti-Inflammatory Drug for Implantable Medical Devices. *Biomaterials* **2002**, 23 , 1649-1656.

47. Tsurufuji, S.; Sugio, K.; Takemasa, F. The Role of Glucocorticoid Receptor and Gene Expression in the Anti-Inflammatory Action of Dexamethasone. *Nature* **1979**, 280, 408-410.

48. Salvador, E.; Shityakov, S.; Förster, C. Glucocorticoids and Endothelial Cell Barrier Function. *Cell Tissue Res.* **2014**, 355, 597-605.

49. Liang, C. C.; Park, A. Y.; Guan, J. L. In Vitro Scratch Assay: a Convenient and Inexpensive Method for Analysis of Cell Migration In Vitro. *Nat. Protoc.* **2007**, 2, 329-333.

50. Roos, D.; Law, S. K. Hematologically Important Mutations: Leukocyte Adhesion Deficiency. *Blood Cells Mol. Dis.* **2001**, 27, 1000-1004.

51. Ley, K.; Laudanna, C.; Cybulsky, M. I.; Nourshargh, S. Getting to the Site of Inflammation: the Leukocyte Adhesion Cascade Updated. *Nat. Rev. Immunol.* **2007**, 7, 678-689.

52. Cronstein, B. N.; Kimmel, S. C.; Levin, R. I.; Martiniuk, F.; Weissmann, G., A Mechanism for the Antiinflammatory Effects of Corticosteroids: the Glucocorticoid Receptor Regulates Leukocyte Adhesion to Endothelial Cells and Expression of Endothelial-Leukocyte Adhesion Molecule 1 and Intercellular Adhesion Molecule 1. *Proc. Natl. Acad. Sci.U. S. A.* **1992**, 89, 9991-9995.

53. Mulligan, M. S.; Varani, J.; Dame, M. K.; Lane, C. L.; Smith, C. W.; Anderson, D. C.; Ward, P. A., Role of Endothelial-Leukocyte Adhesion Molecule 1 (ELAM-1) in Neutrophil-Mediated Lung Injury in Rats. *J. Clin. Invest.* **1991**, 88, 1396-1406.

54. Iademarco, M. F.; Barks, J. L.; Dean, D. C. Regulation of Vascular Cell Adhesion Molecule-1 Expression by IL-4 and TNF-alpha in Cultured Endothelial Cells. *J. Clin. Invest.* **1995**, 95, 264-271.

55. Lee, W. C.; Bhagat, A. A. S.; Huang, S.; Van Vliet, K. J.; Han, J.; Lim, C. T. High-throughput Cell Cycle Synchronization Using Inertial Forces in Spiral Microchannels. *Lab Chip* **2011,** 11, 1359-1367.

Table of Contents Graphic